Journal of Hazardous Materials 171 (2009) 739–747

Contents lists available at ScienceDirect

Journal of Hazardous Materials

journal homepage: www.elsevier.com/locate/jhazmat

Hazardous gas dispersion: A CFD model accounting for atmospheric stability classes

M. Pontiggia, M. Derudi, V. Busini, R. Rota*

Politecnico di Milano, Dipartimento di Chimica, Materiali, Ingegneria Chimica "Giulio Natta", via Macinelli 7, 20131 Milano, Italy

ARTICLE INFO

Article history:
Received 21 November 2008
Received in revised form 15 June 2009
Accepted 15 June 2009
Available online 21 June 2009

Keywords:
CFD
Turbulence modelling
Gas dispersion
Atmospheric stability
Safety

ABSTRACT

Nowadays, thanks to the increasing CPU power the use of Computational Fluid Dynamics (CFD) is rapidly imposing also in the industrial risk assessment area, replacing integral models when particular situations, such as those involving complex terrains or large obstacles, are involved. Nevertheless, commercial CFD codes usually do not provide specific turbulence model for simulating atmospheric stratification effects, which are accounted of by the integral models through the well-known stability-class approach. In this work, a new approach able to take account of atmospheric features in CFD simulations has been developed and validated by comparison with available experimental data.

1. Introduction

Risk assessment of hazardous gas releases is an important task in the process industry safety, since this type of scenario can lead to large consequences: the cloud of hazardous products can be carried by wind even for kilometres maintaining its concentration high enough to represent a hazard both for environment and human health. Dense gas clouds, which are characterized by a negative buoyancy, maximize the dangerous effects both in terms of distance and duration of the hazardous clouds since they fall to the ground, where wind speed decreases and the dilution with air is reduced. A hazardous gas release can behave like a dense gas for several, often concurring, reasons: the high molecular weight of the substance (which makes the gas cloud denser than air even at atmospheric conditions), the low temperature, or the presence of aerosols.

The interest in this kind of analysis has brought, in the early 1980s, to the execution of large-spill trials and to the development of simulation mathematical models that are currently used for loss prevention purposes in chemical and process industries [1,2]. Some of them, like DEGADIS, SLAB, ALOHA and UDM are among the most popular and widely used models in safety engineering applications [3,4]. These are lumped-parameters mathematical models, usually one-dimensional, and account of some physical phenomena using semi-empirical relations whose coefficients have been tuned on field test data (for example, the obstacles geometry is summarized in a couple of parameters, the surface roughness and displacement height) [5]. Outside the range of the experimental data over which these models have been tuned, their reliability is not guaranteed. Since the experimental set-up of the field trials usually does not involve any relevant obstacle, these models consequently provide reliable results only in open field conditions.

In order to simulate more complex geometries and to analyze the effect of large obstacles on gas dispersion, computational fluid dynamic methods have been applied. This approach allows for performing a full three-dimensional analysis, and to predict velocity, temperature, and concentration fields. While assuring more detailed results, it requires a larger amount of resources both in terms of CPU time and analyst skill. CFD results have been successfully validated against experimental field data [6], lab scale trials [7] and they have been also used for complex geometries analysis, such as urban canyons [8].

However, particular attention in CFD simulations has to be paid to turbulence modelling. The effect of the turbulent fluctuations can be modelled through the RANS (Reynolds Averaged Navier–Stokes) approach, or fully simulated through Direct Numerical Simulation (DNS). The DNS is very resources demanding and, nowadays, can be applied only to very simple cases. An intermediate solution is represented by Large Eddies Simulations (LES) that simulate only the larger eddies and use models for simulating the effects of isotropic dissipating eddies. Although LES is less demanding than DNS, it is still quite demanding in complex scenarios. Consequently, RANS still represents a good compromise between results accuracy and computational efforts. The most popular closure model for the

* Corresponding author. Fax: +39 0223993180.
E-mail address: renato.rota@polimi.it (R. Rota).

0304-3894/$ – see front matter © 2009 Elsevier B.V. All rights reserved.
doi:10.1016/j.jhazmat.2009.06.064

RANS approach is the k–ε two-equations model, since it assures reasonable results and good stability [9].

RANS-CFD models are currently implemented in commercial codes, which are multi-tasking instruments mainly developed for confined flow simulations (for example, flow inside pipes or mixers) or for external aerodynamic simulations (such as lift and drag wing forces). As a consequence, only few efforts have been devoted to complement commercial CFD codes with models for the closure of the RANS approach specific for the atmospheric boundary layer analysis, which are not yet available as standard tools (see for instance the work by Hanna et al. [10]). Moreover it is well known that standard k–ε model in some atmospheric conditions tends to over predict pollutants concentration in the far field.

A few theoretical works have been carried out to investigate the possibility of including atmospheric turbulence effects in CFD simulations. Riddle et al. [11] demonstrated that the k–ε model can not maintain the boundary conditions established accordingly to the Monin–Obukhov profiles even in open field simulations: without any external influence, velocity, temperature, turbulent kinetic energy (k), and turbulent dissipation rate (ε) change over the domain. A seven-equations closure model was also provided in order to achieve consistency between CFD simulations and Monin–Obukhov theory. To ensure the consistency between Monin–Obukhov theory and CFD predictions, Hargraves and Wright [12] and Blocken et al. [13] developed a wall-law modification for representing the wall roughness effect in the k–ε model for neutral atmospheric stratification. This solution enhances the previous results but still does not provide stable profiles over a flat terrain.

Other works focused on the turbulence generated by obstacles within the domain, but paid almost no attention to atmospheric stability consistency [14,15] since they eventually provide initial profiles that are substantially changed by the presence of obstacles [16,17].

Finally, some works developed new atmospheric-specific closure models [18] or changed k–ε constants to achieve a better agreement with atmospheric profiles [19,20]. Even if they lead to reasonable predictions for atmospheric turbulence in open field, these models are not validated for other kinds of turbulence, such as that arising from the interaction with obstacles.

In this work, a two-equations turbulence model able to ensure consistency between the Monin–Obukhov theory and CFD predictions has been developed. It couples the advantage of the seven-equations model (that is, the ability of providing stable profiles over a flat terrain) with those of the standard k–ε model (that is, less boundary conditions and faster and more robust numerical solutions) and its performances have been compared with both experimental data and standard k–ε model predictions.

More precisely, a new methodology (named ASsM, Atmospheric Stability sub-Model) for including the effects of atmospheric stratification on dense gas dispersion CFD simulations has been developed. Heavy gases have been considered since they represent the worst case scenario when dealing with safety problems. Moreover, neutral and stable atmospheric stratification (D and F stability classes), which are commonly used in risk assessment when dealing with hazardous gas dispersion, have been considered. Moreover, suitable boundary conditions have been used for both inlet and ground surface to include atmospheric turbulence effects. The proposed ASsM approach is simple, not CPU demanding and stable enough to be used for engineering computations.

2. Theoretical background

Along with Navier–Stokes Eqs. (1) and (2), CFD codes solve specific model equations, such as energy balance (3), species diffusion, turbulence, etc.

$$\frac{\partial \rho}{\partial t} + \nabla \cdot (\rho \vec{v}) = 0 \tag{1}$$

$$\frac{\partial}{\partial t}(\rho \vec{v}) + \nabla \cdot (\rho \vec{v}\vec{v}) = -\nabla p + \nabla \cdot \left(\bar{\bar{\tau}}\right) + \rho \vec{g} \tag{2}$$

$$\frac{\partial(\rho c_v T)}{\partial t} + \nabla \cdot (\rho \vec{v} c_p T) = \nabla \cdot (k_T \nabla T) \tag{3}$$

In the equation above ρ is the density, t the time, v the velocity, p the pressure, τ the shear stress, g the gravity acceleration, c_v and c_p the specific heats, T the temperature and k_T the thermal conductivity.

In this work the k–ε model has been used for representing the effects of the turbulence. This model introduces two additional transport equations for turbulent kinetic energy k (4) and turbulent kinetic energy dissipation rate ε (5), respectively [21]:

$$\frac{\partial}{\partial t}(\rho k) + \frac{\partial}{\partial x_i}(\rho k u_i) = \frac{\partial}{\partial x_j}\left[\left(\mu + \frac{\mu_T}{\sigma_k}\right)\frac{\partial k}{\partial x_j}\right] + G_k + G_b - \rho\varepsilon - Y_M \tag{4}$$

$$\frac{\partial}{\partial t}(\rho \varepsilon) + \frac{\partial}{\partial x_i}(\rho \varepsilon u_i) = \frac{\partial}{\partial x_j}\left[\left(\mu + \frac{\mu_T}{\sigma_\varepsilon}\right)\frac{\partial \varepsilon}{\partial x_j}\right] + C_{\varepsilon 1}\frac{\varepsilon}{k}(G_k + C_{\varepsilon 3} G_b) - C_{\varepsilon 2}\rho\frac{\varepsilon^2}{k} \tag{5}$$

where u_i is the velocity component along x_i direction, μ the viscosity, μ_T the turbulent viscosity, G_k the shear stress-related turbulent kinetic energy production (6), G_b the buoyancy-related turbulent kinetic energy production (7), Y_M the compressibility-related kinetic energy production.

$$G_k = -\rho \overline{u_i' u_j'} \frac{\partial u_j}{\partial x_i} \tag{6}$$

$$G_b = \beta g_i \frac{\mu_t}{\mathrm{Pr}_t}\frac{\partial T}{\partial x_i} \tag{7}$$

In Eqs. (6) and (7) β is the coefficient of thermal expansion, g_i is the component of the gravitational vector along x_i, Pr_t is the turbulent Prandtl number for energy and T the temperature. $C_{\varepsilon 1}$, $C_{\varepsilon 2}$, $C_{\varepsilon 3}$, σ_k, σ_ε, and C_μ are empirical constants. Jones and Launder [22] values have been used for all the k–ε model constants (see Table 1). The commercial package Fluent 6.2.16 [21] has been used for all the computations.

Table 1
k–ε Model constants [22].

$C_{\varepsilon 1}$	$C_{\varepsilon 2}$	$C_{\varepsilon 3}$	σ_k	σ_ε	C_μ
1.44	1.92	1.0	1.0	1.3	0.09

3. Boundary conditions and source terms for representing different atmospheric stability classes

In order to validate the proposed methodology, at first Prairie Grass experiments [23] have been used. These involve continuous releases of small amount of sulphur dioxide at or near ground level over a flat terrain. The experiments were carried out during both day and night times leading to a wide range of atmospheric stability conditions (see Table 2). Concentration values of sulphur dioxide were measured from an array of sensors located at downwind distances of 50, 100, 200, 400 and 800 m. Among all the experiments, in this work only those involving neutral and stable stratifications have been considered since these atmospheric conditions are the most used when assessing the consequences of industrial accidents. Unstable conditions raise the atmospheric turbulence and, therefore, the dilution of the released gas, thus

Table 2
Experimental set-up for Prairie Grass test [23].

	PG 13	PG 17	PG 34	PG 41	PG 58
Release rate [kg s^{-1}]	0.0611	0.0565	0.0974	0.0399	0.0405
Release velocity [m s^{-1}]	11.1	10.5	18.4	7.3	7.5
Stability class	F	D	D	E	F
Wind speed (z = 2 m) [m s^{-1}]	1.3	3.3	9	4	1.9
Ambient temperature [K]	293.15	300.15	304.15	294.15	299.15
Monin–Obhukov length [m]	9	∞	∞	21	9
U_* [m s^{-1}]	0.0789	0.239	0.651	0.267	0.115
T_* [K]	0.0491	–	–	0.240	0.107

reducing the zone interested by hazardous gas concentration and leading to less severe consequences.

Moreover, in order to check the performances of the ASsM approach when obstacles are present, a test from the Falcon test series has been also simulated. These tests involve LNG spills onto a rectangular water pond (60 m long and 40 m wide provided with impoundment walls [24]) from four pipes, fitted with 0.11 m orifices to maximize the LNG pool dimension. The vapor fence is approximately 8.7 m height and extends upwind, enclosing a total area of 88 m long and 44 m wide. In addition to this fence, a billboard 13.3 m tall and 17.1 m wide is located upwind of the water pond. Falcon test 1 has been selected since it involves a stable stratification where atmospheric turbulence reduction is more important and consequently the atmospheric turbulence model ASsM proposed in this work plays a major role. Moreover, literature data obtained using the Reynolds Stress Model (RSM) for this test are available as a reference [25].

Through preliminary CFD simulations of these experiments carried out using constant profiles for wind velocity, air temperature, turbulent kinetic energy and turbulent dissipation rate as inlet boundary conditions for the wind inlet, it has been verified that, even in open field, the vertical profiles of these variables change drastically throughout the integration domain. This is due to two opposing effects: a progressive rise of turbulence intensity near the ground produced by the terrain roughness, and a quick disappearance of turbulent intensity away from ground due to the lack of shear stress in the flat-profile air flow. These changes in the profiles mean that the air flow is not fully developed. This is a problem since, when performing atmospheric open field steady-state simulations, wind is expected to behave as a fully developed flow and the vertical profiles of temperature, velocity and turbulence must be representative of the atmospheric physics for predicting correctly the gas dispersion.

In order to describe the atmospheric flow over uniform flat terrain, the turbulent viscosity can be expressed as a function of the mixing length relation through the Monin–Obukhov similarity theory [26]:

$$\mu_T(z) = \frac{\rho K u_* z}{\Phi_m(z/L)} \tag{8}$$

where $K = 0.42$ is the von Karman constant, u_* the turbulent friction velocity, z the vertical coordinate ($z = 0$ at ground), Φ_m a function that depends on z, and L, the Monin–Obukhov length. For neutral and stable stratification $\Phi_m = 1 + 5(z/L)$.

The Monin–Obukhov length is an estimation of the height where the turbulent dissipation due to the buoyancy is comparable with the shear stress production of turbulence and it can be expressed by the following relation [26]:

$$L = \frac{u_*^2 T_w}{K g T_*} \tag{9}$$

The turbulent friction velocity, u_*, and temperature, T_*, are defined as:

$$u_* = \sqrt{\frac{\tau_w}{\rho}} \tag{10}$$

$$T_* = \frac{-\dot{q}_w}{\rho c_P u_*} \tag{11}$$

where τ_w is the surface shear stress, T_w the surface temperature, q_w the surface heat flux, and g the gravitational acceleration module.

Assuming the shear stress and heat flux constant over the lower part of the atmospheric boundary layer, modified logarithmic velocity and temperature profiles for stable stratification can be obtained [26]:

$$u = \frac{u_*}{K}\left[\ln\left(\frac{z}{z_0}\right) + \Phi_m\left(\frac{z}{L}\right) - 1\right] \tag{12}$$

$$T(z) - T_w = \frac{T_*}{K}\left[\ln\left(\frac{z}{z_0}\right) + \Phi_m\left(\frac{z}{L}\right) - 1\right] - \frac{g}{c_p}(z - z_0) \tag{13}$$

where z_0 is the roughness length of the site. Measuring u, T at a given quote z, T_w and z_0, it is possible, through Eqs. (12) and (13), to evaluate u_* and T_*.

In this work, the approximation of incompressible gas has been retained for air, as usual in this kind of simulations, since it leads to a faster and more robust numerical solution without a sensible loss of information. Therefore it is not possible to balance the adiabatic profile of temperature (13) varying the pressure along z-direction. As a consequence, a reduced temperature has been implemented as boundary conditions at the wind inlet:

$$\theta = T(z) + \frac{g}{c_p}(z - z_0) = T_w + \frac{T_*}{K}\left[\ln\left(\frac{z}{z_0}\right) + \Phi_m\left(\frac{z}{L}\right) - 1\right] \tag{14}$$

While velocity and temperature profiles can be directly imposed as boundary conditions, turbulent viscosity is evaluated by the k–ε model as a function of turbulent kinetic energy and turbulent dissipation rate. Therefore, proper profiles for the turbulence variables must be obtained in order to have consistency between CFD computed values of μ_T and the values provided by the Monin–Obhukov similarity (Eq. (8)). The consistency between Monin–Obhukov profiles and k–ε model predictions is necessary to assure constant (that is, fully developed) vertical profiles throughout the integration domain in open field simulations.

3.1. Neutral stratification

For neutral stratification, the heat flux from the ground is equal to zero. Therefore the Monin–Obukhov length is infinite and Φ_m goes to 1, the friction temperature T_* goes to zero, and the reduced temperature is constant along the vertical (z) direction. Assuming flat profile for the kinetic energy [26] and rearranging the transport equations of turbulent kinetic energy (4) in steady-state conditions with Eqs. (8) and (12), over flat terrains (i.e., with no gradients along x and y directions) we can find:

$$\varepsilon(z) = \frac{u_*^3}{Kz} \tag{15}$$

$$k = \frac{u_*^2}{\sqrt{C_\mu}} \tag{16}$$

Eqs. (15) and (16) are mathematically consistent with k transport equation; in order to assure the consistency also with turbulent dissipation rate equation, Alinot and Masson [19] suggested to change the k–ε model constants. However, this solution, while leading to good performances for the evaluation of atmospheric profiles, has not been validated against atmospheric gas dispersion experiments. Consequently, the addition of a z-dependent source term,

S_ε, to the ε transport equation has been preferred in this work. This term can be obtained through the substitution of the profiles (15) and (16) in Eq. (5), with the assumptions of two-dimensional flow with zero vertical velocity, steady state, constant pressure and shear stress, leading to:

$$S_\varepsilon(z) = \frac{\rho u_*^4}{z^2}\left[\frac{(C_{\varepsilon 2} - C_{\varepsilon 1})\sqrt{C_\mu}}{K^2} - \frac{1}{\sigma_\varepsilon}\right] - \mu\frac{u_*^3}{2Kz^3} \tag{17}$$

This equation represents a source term of the turbulent dissipation rate due to some atmospheric features that the standard k–ε model can not reproduce, since the standard k–ε model equations are not consistent with Monin–Obukhov profiles. Moreover, since this term is added to all the other turbulence source contributions (e.g., gas expansion, jet propagation, interaction with obstacles, ...) the resulting equation:

$$\frac{\partial}{\partial t}(\rho\varepsilon) + \frac{\partial}{\partial x_i}(\rho\varepsilon u_i) = \frac{\partial}{\partial x_j}\left[\left(\mu + \frac{\mu_T}{\sigma_\varepsilon}\right)\frac{\partial \varepsilon}{\partial x_j}\right] + C_{\varepsilon 1}\frac{\varepsilon}{k}(G_k + C_{\varepsilon 3}G_b) - C_{\varepsilon 2}\rho\frac{\varepsilon^2}{k} + S_\varepsilon(z) \tag{18}$$

is expected to be able to represent the simultaneous effect of all these contributions.

It should be noted that S_ε is composed by two terms: the former contains all the dependences on k–ε model constants, while the latter depends on molecular viscosity. Neglecting this second term, it is possible to obtain the relations used by Alinot and Masson [19] for the evaluation of their new constants.

3.2. Stable stratification

In stable stratification Φ_m does not tend to 1 and temperature is not constant. Therefore, the procedure discussed previously for neutral conditions becomes more complex. Considering again a flat k-profile (that is, neglecting the diffusion terms in Eq. (4)) and following the same procedure discussed in section 3.1 turbulent profiles can be obtained for both k and ε:

$$\varepsilon = \frac{u_*^3}{Kz}\Phi_\varepsilon \tag{19}$$

$$k = \frac{u_*^2}{\sqrt{C_\mu}}\sqrt{\frac{\Phi_\varepsilon(z/L)}{\Phi_m(z/L)}} \tag{20}$$

where Φ_ε is a function similar to Φ_m, as proposed by Panofsky and Dutton [26]:

$$\Phi_\varepsilon = \left(1 + 4\frac{z}{L}\right) \tag{21}$$

Turbulent kinetic energy (20) depends on z and consequently, in this case, it is not possible to neglect the diffusion term without introducing an identical but opposite source term in the k Eq. (4):

$$S_k = -\frac{\partial}{\partial z}\left[\left(\mu + \frac{\mu_T}{\sigma_k}\right)\frac{\partial k}{\partial z}\right] \tag{22}$$

However, it can be noted from Eq. (20) that the k dependence on z is quite negligible since k tends rapidly to a constant value. Consequently, its derivative in Eq. (22) is close to zero and the S_k term can be safely neglected without any significant loss of accuracy. Simulations have been performed both with and without the S_k term, and it has been verified that including this source term increases the computational efforts without any significant improvement in the vertical profiles prediction.

Following the same procedure discussed for neutral stratification, an equation for S_ε has to be obtained in order to assure k–ε model consistency with the Monin–Obhukov similarity theory, leading to the following relation:

$$S_\varepsilon(z) = \frac{u_*^4\rho}{z^2}\left[\frac{(C_{\varepsilon 2} - C_{\varepsilon 1})\sqrt{C_\mu}}{K^2}\Phi_\varepsilon^2\sqrt{\frac{\Phi_\varepsilon}{\Phi_m}} - \frac{1}{\sigma_\varepsilon}\left(\frac{2}{\Phi_m} - \frac{1}{\Phi_m^2} + \frac{T_*}{KT}\right)\right] - \mu\frac{2u_*^3}{Kz^3} \tag{23}$$

Also in this case S_ε is composed by two terms; the molecular viscosity-dependent term remains unchanged, while the first one becomes much more complex.

3.3. Wall treatment

The shear stress turbulence production is particularly important near the ground; CFD codes usually model the laminar region near walls using a logarithmic velocity profile:

$$\frac{u u_*}{\tau_w/\rho} = \frac{1}{K}\ln\left(\frac{E\rho u_* x_j}{\mu}\right) - \Delta B \tag{24}$$

where τ_w is the shear stress, E an empirical constant ($E = 9.793$), μ the molecular viscosity, ΔB a roughness-dependent correction. Varying the roughness effects on fluid motion, it is possible to define three different regions, which provide different equations for the velocity profile correction term [22]:

$$\begin{aligned} &K^+ \le 2.25 \rightarrow \Delta B = 0 \\ &2.25 \le K^+ \le 90 \\ &\rightarrow \Delta B = \frac{1}{K}\ln\left(\frac{K^+ - 2.25}{87.75} + C_S K^+\right)^{\sin(0.4258[\ln K^+ - 0.811])} \\ &K^+ > 90 \rightarrow \Delta B = \frac{1}{K}\ln(1 + C_S K^+) \end{aligned} \tag{25}$$

where $K^+ = \rho K_S u_*/\mu$, K_S is the roughness height, and C_S a constant that depends on the roughness. While K_S should be directly measured, C_S value is hard to foresee: it is equal to 0.5 for fully uniform surface roughness, and tends to 1 for inhomogeneous surface patterns.

Low value of K^+ ($K^+ < 2.25$) means that viscosity rules over turbulent effects and, therefore, ΔB can be neglected. When K^+ is large ($K^+ > 90$), roughness effects become prominent and a ΔB equation should be provided. In atmospheric flows K^+ values are generally high and fully turbulent situation are considered. Anyway, both fully turbulent and intermediate behaviours can be rewritten as:

$$\Delta B = \frac{1}{K}\ln f(K_S, C_S) \tag{26}$$

which, once replaced in Eq. (22), leads to the following velocity profile:

$$u = \frac{u_*}{K}\ln\left(\frac{E\rho u_* x_j}{\mu f(K_S, C_S)}\right) \tag{27}$$

Near the walls the shear stress prevails over buoyancy, and neutral stratification profiles should be considered for velocity. By equating Eqs. (27) and (12), C_S can be implicitly obtained as:

$$\frac{E\rho u_*}{\mu f(K_S, C_S)} = \frac{1}{z_0} \tag{28}$$

Eq. (28) was proposed to evaluate the surface roughness [13], while in this work surface roughness has been considered a known parameter and C_S values have been calculated for all the simulated tests, obtaining a constant value equal to 0.979. This can be considered a suitable value for wall treatment in atmospheric gas dispersion problems since, as mentioned before, a value of C_S close to 1 means inhomogeneous surface, well suited to describe terrain roughness.

Moreover, since in all the simulated experiments surface roughness value is very small (about 6 cm), the dimension of the first cell near the ground can be fixed at about 12 cm (that is, double the surface roughness value) without compromising grid resolution, thus fulfilling Blocken constraints [13].

4. Profiles tuning through periodic simulations

The validation of the proposed approach requires at first to verify that CFD fully developed vertical profiles correctly compare with those arising from the Monin–Obhukov similarity theory. When using CFD codes for simulating atmospheric gas dispersion, usually a long domain upwind the gas release location is required to allow the vertical profiles of all the relevant variables (i.e. velocity, temperature, turbulence intensity, and dissipation rate) to become fully developed (i.e. in agreement with both the BCs and the equations used for the particular situation) starting from the (arbitrary) profiles set as boundary conditions at the wind inlet boundary. This means that a large part of the computational domain is wasted (since it is required only to develop the atmospheric profiles) leading to an unnecessary increase of the CPU time. However, the availability of the correct profiles (i.e. those corresponding to fully developed profiles for a given atmospheric stability class) would allow to avoid the empty domain upwind the gas release location, thus strongly reducing the cell number and consequently CPU time. Therefore, a simple approach involving periodic 2D simulation over flat terrain [9,13,27] and able to easily compute the correct profiles to be set as boundary conditions on the wind inlet boundary has been used in this work. Periodic simulations use conditions obtained at the outlet boundary as an input for the inlet boundary and are provided as standard tools in CFD codes. The lower boundary (the ground) has been represented using a wall boundary, while for the upper boundary a velocity inlet profile has been used. This approach mimes, using a very short domain, a virtually infinite domain thus providing fully developed profiles. Moreover 2D simulations are much less demanding than 3D ones and consequently this approach is definitely no time consuming: these simulations requires only a few minutes to be performed on a single CPU.

Fully developed vertical profiles have to be computed through 2D periodic simulations (and cannot be predicted) since in neutral stratification the constant k value along z direction requires a zero derivative value, while the equations used by the near-wall treatment impose an infinite derivative. Moreover, in stable stratification the S_k term has been neglected. Both these approximations introduce a small inconsistency between the Monin–Obhukov profiles and the profiles predicted by the modified k–ε model, as shown in Figs. 1 and 2.

Using this approach, all the integration domain upwind the first significant item (that can be either the source term or an obstacle) could be theoretically removed from the computational grid. However, since some items can modify significantly also the upwind flow field, a minimum upwind domain is always required. The minimum value of the upwind domain has to be defined case-by-case since it depends on the specific characteristics of the first significant item, and the invariance of the solution when changing the extension of the upwind domain has to be verified. In this study, for each investigated run the results obtained using at least two different computational grids and two different upwind integration domain dimensions have been compared to verify the invariance of the results when changing these parameters.

Figs. 1 and 2 show the overall results of this analysis comparing the profiles required by the Monin–Obhukov similarity theory and those predicted by CFD computations for the atmospheric conditions of two Prairie Grass experimental tests, namely PG 13 and PG 17 (see Table 2). These tests are characterized either by neutral or very stable stratification.

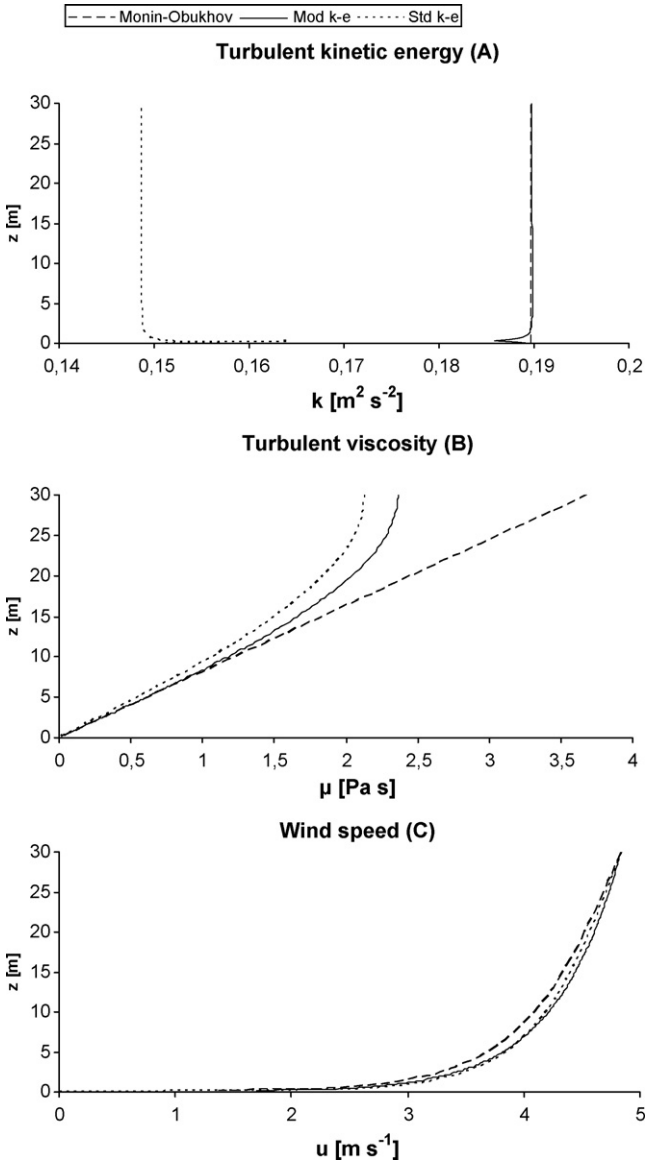

Fig. 1. 2D periodic simulation results for PG-17 test with neutral stratification.

Comparing the vertical profiles shown in Figs. 1 and 2, we can see that in neutral conditions (where the atmospheric turbulence is larger) the turbulent viscosity value increases almost linearly along z (accordingly with Eq. (8)), reaching a value of about 4 Pa s at the top of the domain, while in stable conditions (where the atmospheric turbulence is smaller) the μ_T profile is altered by the Φ_m contribution and its maximum value is about 0.8 Pa s. This means that, as expected, stable stratification reduces turbulent viscosity and consequently atmospheric turbulence. Wind speed profiles reflect turbulent viscosity profiles: higher viscosity means more uniform wind speed, while low viscosity means larger velocity gradient.

We can see from Figs. 1 and 2 that there is a good agreement between the profiles required by the Monin–Obhukov similarity theory and those predicted by CFD computations when implementing the proposed ASsM approach. However, we can also see that increasing the height above ground, the effect of the upper boundary (that have been set as velocity inlet, with the air velocity tangential to the boundary surface itself) actually interferes in turbulent viscosity determination: while ensuring the right velocity value, this boundary brings to zero the flux of turbulent kinetic energy and turbulent dissipation rate. This problem can be eas-

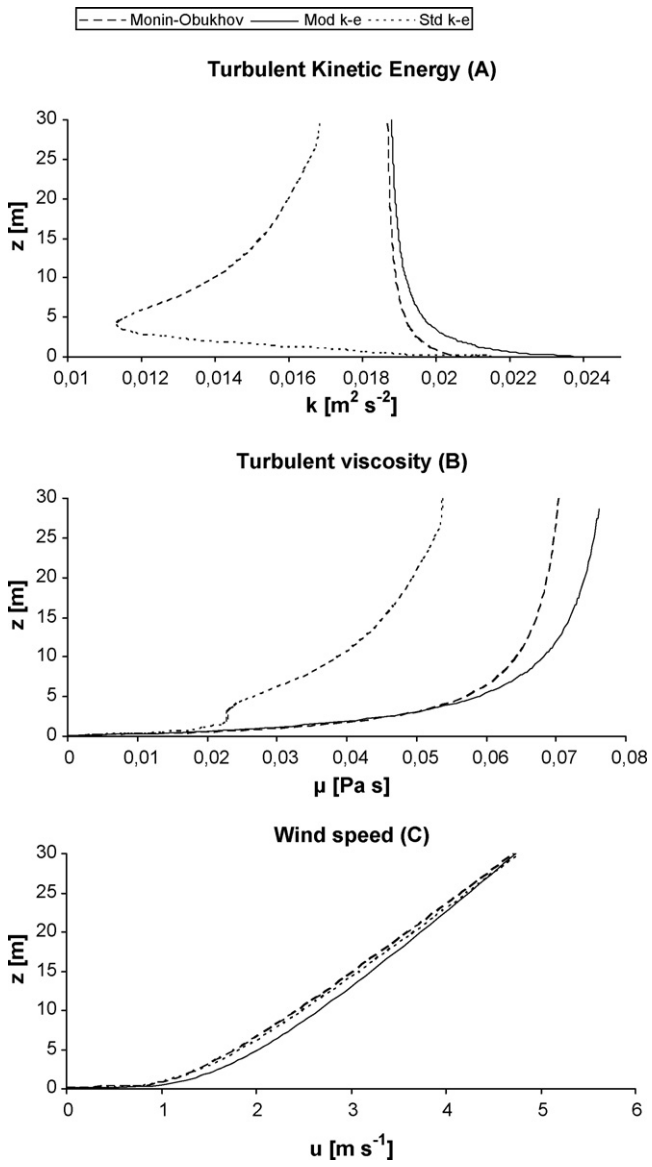

Fig. 2. 2D periodic simulation results for PG-13 test with stable stratification.

ily faced by setting, as usual, a domain high enough to avoid this interference in the cloud region. For instance, in the investigated gas releases the SO_2 clouds height never exceeded 5 m above ground, where turbulence predictions are still acceptable. As a rule of thumbs, a domain height at least double than the maximum cloud height should be used in practical CFD computations over flat terrains.

We can also see that in neutral stratification the wall-boundary condition of infinite derivative set by the CFD code as wall-type boundary condition is well absorbed close to the ground, and the whole profile can be considered reasonably flat. Moreover, the good agreement found also in stable stratification conditions means that the approximation of neglecting the S_k term does not influence significantly the vertical profiles determination, while providing a considerable improvement of the solution stability.

Finally, Figs. 1 and 2 also report the results of the same CFD computations performed using the standard k–ε model. The large improvement obtained using the developed approach is quite evident.

The k, ε, and v profiles obtained from 2D periodic simulations have been imported in fully 3D simulations over a flat terrain, and it has been verified that they remain unchanged in the whole integration domain.

Table 3
Boundary conditions used in all the simulations.

Boundary	Type	Notes
Wind Inlet boundary	Velocity inlet	Wind velocity, temperature and turbulence values for the wind inlet flux
Wind Outlet boundary	Pressure outlet	Constant pressure outlet surface
Top boundary	Velocity inlet	Wind velocity, tangential to the surface
Symmetry boundary	Symmetry	Zero derivative value for all the variables
Lateral boundary	Velocity inlet	Wind velocity, tangential to the surface
Ground boundary	Wall	No-slip conditions, roughness specification, fixed temperature
Gas inlet boundary	Mass flow inlet	Mass flow, temperature and turbulence values for the gas inlet flux

5. Comparison with experimental data

Simulations of the SO_2 releases summarized in Table 1 have been performed and the results have been compared with the available experimental data, that is, gas concentration at 1.5 m above ground at the plume centre for several distances downwind. Since SO_2 was released in open field, the scenario has a symmetry plane. This allows imposing symmetry boundary conditions on this plane in order to simulate only a half of the domain with lower computational efforts. The computational domain is about 800 m long, 30 m high and 50 m wide and a first attempt mesh counts about 700k elements. After some preliminary simulations, the mesh has been adapted case-by-case with a selective mesh refinement: only a cluster of grid elements covering the cloud region has been selected and refined. This approach saves a large number of elements in comparison with the refinement of the whole domain. Meshes with about 900–1000k elements have been obtained in this way and the results have been proved to be grid-independent. The boundary conditions used in all the simulations are summarized in Table 3. Simulations using the final mesh required about 5 h on a workstation node equipped by two Opteron 64 bit CPUs.

Figs. 3–5 show the comparison between experimental data and predicted concentration profiles at 1.5 m above the ground for each field test considered.

As summarized in Table 2, the experimental data refer to very different weather conditions, with wind speed raging from 1 m s^{-1} to about 10 m s^{-1}, and neutral, stable and very stable stratifications. Despite this wide range of atmospheric conditions, there is a good agreement between model predictions and experimental data, even where only long distance (1000 m) and, therefore, low concentration (10 ppm), data are available. This means that the proposed approach is able to reproduce correctly the influence of the atmospheric stability class on gas dispersion. It should be stressed that the results summarized in Figs. 3–5 are true model predictions, that is, no model parameters have been tuned against the experimental data.

Moreover, since the ASsM approach requires fully developed profiles as boundary conditions at the wind inlet boundary obtained through 2D periodic simulations, it has been possible to locate the source term near the inlet boundary, thus avoiding the simulation of the upwind domain required to allow the k, ε, T, and v vertical profiles to fully develop. This is especially useful when geometrical complexity leads to large grid dimension, and a reduction of

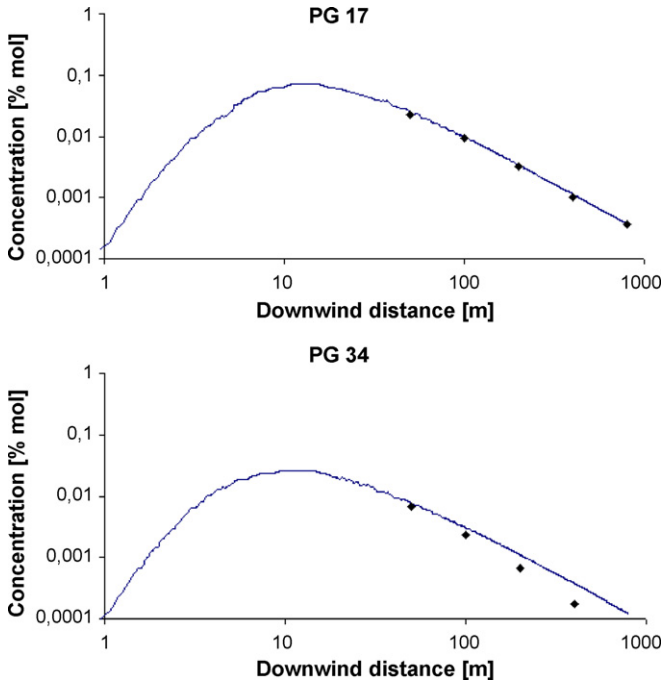

Fig. 3. Comparison between field tests experiments (♦) and CFD model predictions with the modified k–ε model (—); stability class D, neutral stratification.

the number of elements is especially appreciated. However, in geometrically complex terrains it could be necessary to simulate some upwind domain where significant obstacles are present in order to correctly reproduce the flow field upwind the source term.

From the results shown in Figs. 3–5 it can be noted that in neutral stratification the SO_2 concentration reaches a value of 10^{-4} mol% 1 m downwind the release point, while in stable stratification this concentration is reached at about at 1.3 m downwind and in very stable stratification at 1.7 m. This is due to the lateral spreading of the SO_2 jet, which is influenced by the atmospheric turbulence: a more turbulent stability class (D) means larger air entrainment and consequently a faster lateral spreading of the jet. Also this feature is well predicted by the proposed model, as shown in Fig. 6 where iso-concentration profiles of SO_2 on the vertical symmetry plane for three different stability class are reported. The faster the lateral spreading is, the sooner the iso-concentration profile reaches an elevation above the ground of 1.5 m.

The improvement of the ASsM approach can be fully appreciated from the results summarized in Fig. 7, where CFD predictions obtained using the standard k–ε model are also reported. We can see that the well-known problem of a large overestimation of the hazardous distances far downwind the release point is completely

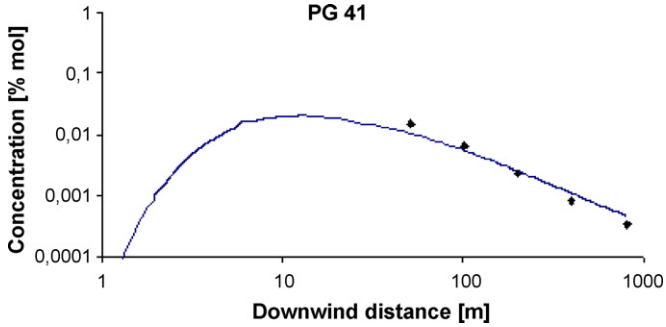

Fig. 4. Comparison between field tests experiments (♦) and CFD model predictions with the modified k–ε model (—); stability class E, stable stratification.

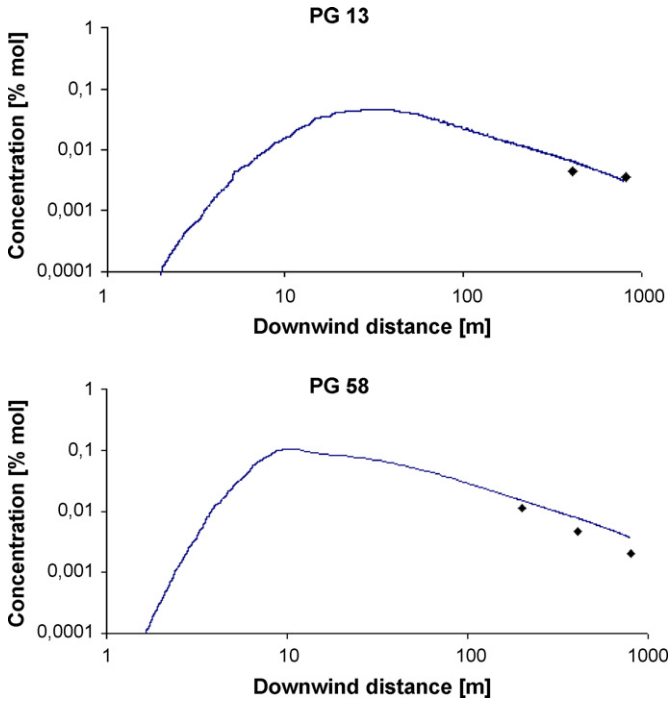

Fig. 5. Comparison between field tests experiments (♦) and CFD model predictions with the modified k–ε model (—); stability class F, very stable stratification.

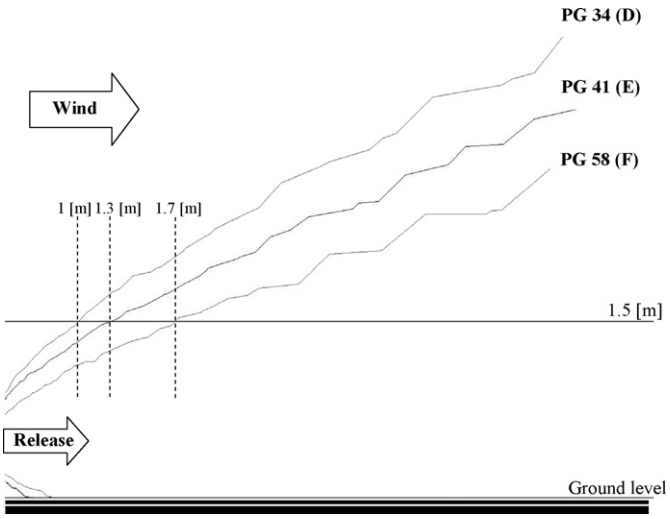

Fig. 6. Iso-concentration (10^{-4} mol%) curves on the vertical symmetry plane for three different stability classes.

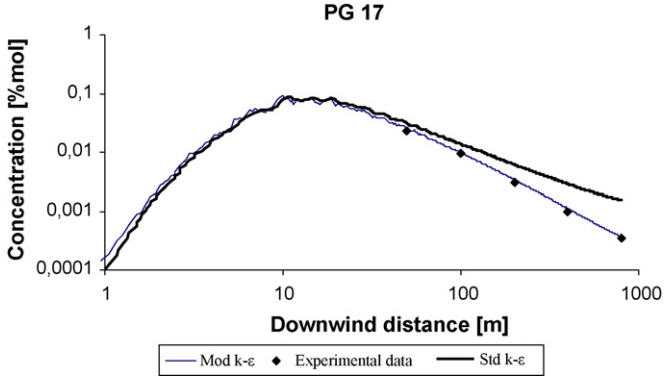

Fig. 7. Comparison between field tests experiments (♦), CFD model predictions with the modified k–ε model (by means of the ASsM approach) (—) and CFD model prediction with the standard k–ε model (—); stability class D, neutral stratification.

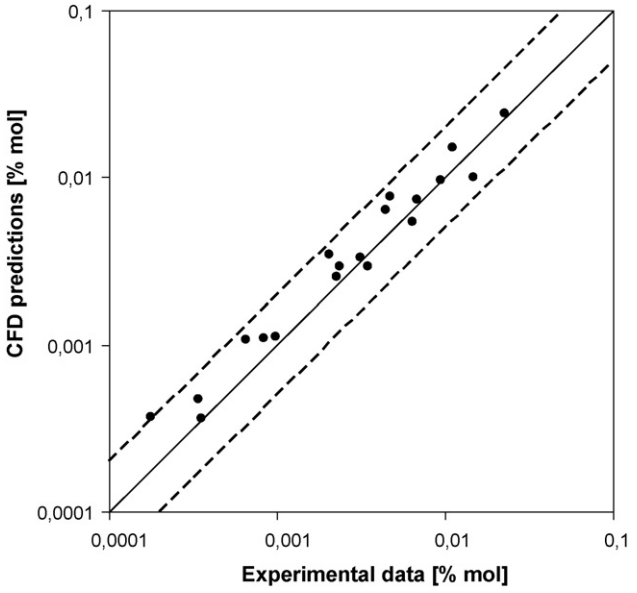

Fig. 8. Parity plot of the modified CFD model predictions vs. experimental data. Dashed lines delimitate the region where the error is lower than a factor of 2, that is $C_{exp}/2 < C_{CFD} < 2\,C_{exp}$.

avoided using the proposed approach; for instance at 1000 m downwind the standard k–ε model overestimates the experimental gas concentrations of about one order of magnitude, while the ASsM approach shows a quite good agreement with the experimental data.

All the obtained results are summarized in Fig. 8, where a plot of CFD previsions versus experimental data is reported. We can see that the proposed approach is able to predict the experimental measurement within a factor of 2. This means that the ASsM approach allows for an accurate prediction of the gas concentrations all over the computational domain; this information is needed not only for toxic gas releases (such as SO_2 releases) but also for flammable gas releases, since it permits to track the zone within the flammability limits. Moreover, since transient simulations can also be performed, it is possible to evaluate the toxic dose, based on which physical effects of the toxic cloud are usually calculated. Work is in progress on this last topic.

The same approach discussed for simulating Prairie Grass experiments has been adopted for simulating Falcon 1 test [24] in order to verify the performances of the ASsM approach in the presence of obstacles. The LNG source term has been represented through a mass flow inlet of the gas from the entire surface of the pond using the turbulence parameters already discussed in the literature [25], while the ground and the obstacles have been represented by a wall boundary, with no-slip conditions for velocity. The obstacles have been considered smooth surfaces, i.e., with zero roughness height. Both the experimental set-up and the boundary conditions used in the simulation are summarized in Tables 4 and 5. Fig. 9 shows

Table 4
Experimental set-up for Falcon 1 field test [24].

	Falcon 1
Release rate [$m^3\,min^{-1}$]	28.7
Orifice diameter [m]	0.11
Stability class	F
Wind speed (z = 2 m) [$m\,s^{-1}$]	1.7
Ambient temperature [K]	305.9
Monin–Obhukov length [m]	5
u_* [$m\,s^{-1}$]	0.0604
T_* [K]	0.0408

Table 5
Boundary conditions used for the simulation of Falcon 1 test.

Boundary	Type	Notes
Wind Inlet boundary	Velocity inlet	Wind velocity, temperature and turbulence values for the wind inlet flux
Wind Outlet boundary	Pressure outlet	Constant pressure outlet surface
Top boundary	Velocity inlet	Wind velocity, tangential to the surface
Lateral boundary	Velocity inlet	Wind velocity, tangential to the surface
Ground boundary	Wall	No-slip conditions, roughness specification, fixed temperature
Obstacles	Wall	No-slip conditions, zero roughness, zero thermal flux
Pool	Mass flow inlet	Mass flow, temperature and turbulence values for the gas inlet flux

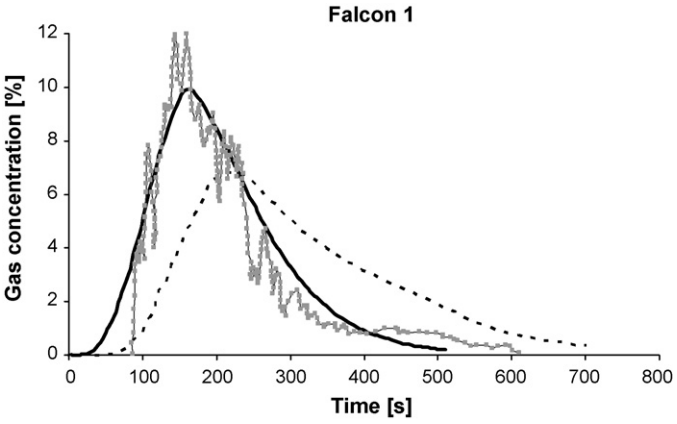

Fig. 9. Comparison between field tests experiments (grey symbols), CFD model predictions with the modified k–ε model developed in this work (ASsM) (black line) and CFD model prediction with the RSM model [25] (dashed line); Falcon 1 test, very stable stratification.

the comparison among the experimental data, the results obtained with the k–ε model modified by means of the ASsM approach developed in this work, and the RSM model previously reported in the literature [25]. This figure shows the gas concentration as a function of time 150 m behind the impoundment and 25 m lateral. A good agreement between the modified k–ε model predictions and the experimental data, with a substantial improvement with respect to the RSM model, has been found.

6. Conclusion

In this work a new approach called ASsM (Atmospheric Stability sub-Model) for the consequences analysis of gas releases in neutral and stable atmospheric stratification through CFD modeling has been proposed. It provides ground wall-type boundary characterization and inlet boundary profiles in agreement with Monin–Obhukov similarity theory through the following steps:

- a source term is added to the ε balance Eq. (5) depending on the stability class as:

$$S_\varepsilon(z) = \frac{\rho u_*^4}{z^2}\left[\frac{(C_{\varepsilon 2} - C_{\varepsilon 1})\sqrt{C_\mu}}{K^2} - \frac{1}{\sigma_\varepsilon}\right] - \mu\frac{u_*^3}{2Kz^3} \quad \text{(neutral stratification)}$$

$$S_\varepsilon(z) = \frac{u_*^4\rho}{z^2}\left[\frac{(C_{\varepsilon 2}-C_{\varepsilon 1})\sqrt{C_\mu}}{K^2}\Phi_\varepsilon^2\sqrt{\frac{\Phi_\varepsilon}{\Phi_m}}-\frac{1}{\sigma_\varepsilon}\left(\frac{2}{\Phi_m}-\frac{1}{\Phi_m^2}+\frac{T_*}{KT}\right)\right] - \mu\frac{2u_*^3}{Kz^3} \quad \text{(stable stratification)}$$

- a value of $C_S = 0.979$ is used in the wall functions for the wall boundary conditions.

Moreover, a procedure to compute k, ε, T and ν vertical profiles at the wind inlet boundary has been suggested. It requires periodic 2D simulations and allows obtaining fully developed profiles, therefore avoiding the simulation of a large empty domain upwind the release point.

The proposed ASsM approach has been successfully validated through the comparison with several different field tests of Prairie Grass series, involving neutral, stable and very stable stratification conditions, and the field test Falcon 1, involving the presence of some obstacles.

Acknowledgements

Financial support of the iNTeg-Risk project (contract number NMP2-LA-2008-213345) of the 7th Framework Programme of the European Commission, as well as that of the Italian MIUR – PRIN2007 is gratefully acknowledged.

References

[1] M. Nielsen, S. Ott, A collection of data from dense gas experiments, RISO Report R-845(EN), RISO, Roskilde, 1996.
[2] S. Hanna, R. Britter, Wind Flow and Vapor Cloud Dispersion at Industrial and Urban Sites, CCPS, New York, 2002.
[3] A. Bernatik, M. Libisova, Loss prevention in heavy industry: risk assessment of large gasholders, J. Loss Prevent. Proc. 17 (2004) 271–278.
[4] D.R. Brook, N.V. Felton, C.M. Clem, D.C.H. Strickland, I.H. Griffiths, R.D. Kingdon, Validation of the Urban Dispersion Model (UDM), Int. J. Environ. Pollut. 20 (2003) 11–21.
[5] J.S. Nordin, Practical uses of air plume modelling in chemical emergencies, in: M. Fingas (Ed.), The Handbook of Hazardous Materials Spills Technology, McGraw-Hill, New York, 2002.
[6] S. Sklavounos, F. Rigas, Simulation of coyote series trials—Part I: CFD estimation of non-isothermal LNG releases and comparison with box-model predictions, Chem. Eng. Sci. 61 (2006) 1434–1443.
[7] M.A. McBride, A.B. Reever, M.D. Vanderheyden, C.J. Lea, X.X. Zhou, Use of advanced techniques to model the dispersion of chlorine in complex terrain, Trans. Inst. Chem. Eng. Part B: Process. Saf. Environ. 79 (2001) 89–102.
[8] R.H. Steven, M.J. Brown, F.E. Camelli, S.T. Chan, W.J. Coirier, O.R. Hansen, A.H. Huber, S. Kim, R.M. Reynolds, Detailed simulations of atmospheric flow and dispersion in downtown Manhattan, an application of five Computational Fluid Dynamics models, B Am. Meteorol. Soc (2006), doi:10.1175/BAMS-87-12-1713.
[9] A. Luketa-Hanlin, R.P. Koopman, D.L. Ermak, On the application of computational fluid dynamics codes for liquefied natural gas dispersion, J. Hazard. Mater. 140 (2007) 504–517.
[10] S.R. Hanna, O.R. Hansen, S. Dharmavaram, FLACS CFD air quality model performance evaluation with Kit Fox, MUST, Prairie Grass and EMU observations, Atmos. Environ. 38 (2004) 4675–4687.
[11] A. Riddle, D. Carruthers, A. Sharpe, C. McHugh, J. Stocker, Comparison between FLUENT and ADMS for atmospheric dispersion modelling, Atmos. Environ. 38 (2004) 1029–1038.
[12] D.M. Hargreaves, N.G. Wright, On the use of the k–ε model in commercial CFD software to model the neutral atmospheric boundary layer, J. Wind Eng. Ind. Aerod. 95 (2007) 355–369.
[13] B. Blocken, T. Stathopoulos, J. Carmeliet, CFD simulation of the atmospheric boundary layer: wall function problems, Atmos. Environ. 41 (2007) 238–252.
[14] S.E. Kim, F. Boysan, Application of CFD to environmental flows, J. Wind Eng. Ind. Aerod. 81 (1999) 145–158.
[15] P. Neofytou, A.G. Venetsanos, D. Vlachogiannis, J.G. Bartzis, A. Scaperdas, CFD simulation of the wind environment around an airport terminal building, Environ. Modell. Softw. 21 (2006) 520–524.
[16] Y. Yang, Y. Shao, Numerical simulations of flow and pollution dispersion in urban atmospheric boundary layers, Environ. Modell. Softw. 23 (2008) 27–40.
[17] H.A. Olvera, A.R. Choudhuri, W.W. Li, Effects of plume buoyancy and momentum on the near-wake flow structure and dispersion behind an idealized building, J. Wind Eng. Ind. Aerod. 96 (2008) 209–228.
[18] L. Cvitan, Classification of the stratified atmospheric boundary layers at Molve (Croatia) based on the similarity theory, Meteorol. Atmos. Phys. 93 (2006) 235–246.
[19] C. Alinot, C. Masson, k–ε Model for the atmospheric boundary layer under various thermal stratification, J. Sol. Energy. 127 (2005) 438–443.
[20] H. Foudhil, Y. Brunet, J.-P. Caltagirone, A fine scale k–ε model for atmospheric flow over heterogeneous landscapes, Environ. Fluid Mech. 5 (2004) 247–265.
[21] Fluent 6 User's Guide, Fluent Inc., Lebanon, 2006.
[22] W.P. Jones, B.E. Launder, The prediction of laminarization with a two-equation model of turbulence, J. Heat Mass Transfer 15 (1972) 301–314.
[23] A. Holt, H.W.M. Witlox, Validation of the unified dispersion model, in: Technical Reference Manual, v. 6.0, DNV, London, 1999.
[24] T.C. Brown, et al., Falcon Series Data Report 1987 LNG Vapor Barrier Verification Field Tests, Gas research Institute Report GRI-89/0138, Contract 5085-252-1189, 1990.
[25] F. Gavelli, E. Bullister, H. Kytomaa, Application of CFD (Fluent) to LNG spills into geometrically complex environments, J. Hazard. Mater. 159 (2008) 158–168.
[26] H. Panofsky, J. Dutton, Atmospheric Turbulence, Wiley, New York, 1984.
[27] F. Scargiali, E. Di Rienzo, M. Ciofalo, F. Grisafi, A. Brucato, Heavy gas dispersion modelling over a topographically complex mesoscale. A CFD based approach, Proc. Saf. Environ. Prot. 83 (2005) 242–256.